coatings

MDPI

Essay

Multi-Method Analysis of Painting Materials in Murals of the North Mosque (Linqing, China)

Shaohua Dong [1], Jiankai Xiang [1], Juan Ji [1], Yongjin Wang [1], Gang Zhang [1], Peng Fu [1], Jianwu Han [1] and Li Li [1,2,*]

[1] Shaanxi Institute for the Preservation of Cultural Heritage, Xi'an 710075, China
[2] School of Cultural Heritage, Northwest University, Xi'an 710127, China
* Correspondence: lili@sxwby.org.cn

Abstract: The murals of Ming Dynasty North Mosque in Linqing, Shandong Province, Eastern China, are of significant cultural and historical importance. Their final restoration date remains uncertain, making a comprehensive investigation critical before initiating preservation and renovation work. This research project examined the painting materials of the murals using various analytical techniques, including polarized light microscopy (PLM), scanning electron microscopy (SEM), X-ray energy spectrometer (EDS), X-ray diffraction (XRD), Fourier transform infrared spectroscopy (FTIR), microscopic Raman spectroscopy (M-Raman), X-ray photoelectron spectroscopy (XPS), and pyrolysis-gas chromatography/mass spectrometry (Py-GC/MS) analysis. Results indicated that the pigments employed included ultramarine, emerald green, cinnabar, kaolinite, gypsum, and carbon black, while the gum binder used was protein-based adhesive materials. As synthetic ultramarine and emerald green were not introduced to China until the late Qing Dynasty, this suggests that these murals were restored no earlier than this period. The study also revealed that the mural materials used in the North Mosque mural were similar to those found in other architectural murals in China. Thus, the knowledge gained from the conservation and restoration efforts of similar architectural murals can be leveraged to enhance the conservation and restoration efforts of the North Mosque murals.

Keywords: emerald green; ultramarine; mural; North Mosque; XPS; Py-GC/MS; XRD; SEM; EDS; Micro-Raman; FTIR

check for updates

Citation: Dong, S.; Xiang, J.; Ji, J.; Wang, Y.; Zhang, G.; Fu, P.; Han, J.; Li, L. Multi-Method Analysis of Painting Materials in Murals of the North Mosque (Linqing, China). *Coatings* **2023**, *13*, 1298. https://doi.org/10.3390/coatings13071298

Academic Editors: Claudia Pelosi, Angela Lo Monaco and Claudia Colantonio

Received: 25 June 2023
Revised: 15 July 2023
Accepted: 20 July 2023
Published: 24 July 2023

Copyright: © 2023 by the authors. Licensee MDPI, Basel, Switzerland. This article is an open access article distributed under the terms and conditions of the Creative Commons Attribution (CC BY) license (https://creativecommons.org/licenses/by/4.0/).

1. Introduction

Since its introduction to China in the 7th century, Islam has continued to spread and develop, with approximately 20 million adherents among 10 ethnic minorities in China [1,2]. The mosque serves as the primary location for Islamic worship, religious education, and missionary activities, and represents a pivotal symbol of Islamic culture. Significantly, a diverse collection of mosques is found throughout China, with many constructions using masonry as a primary building material. The architects employed sophisticated brick and timber techniques to construct numerous mosque buildings [3]. Additionally, the interior decoration of the mosques is distinctly different from traditional Chinese decorative expressions, which have traditionally featured figures or animals painted onto walls for ornamentation. For instance, the famed Mogao Caves, Yungang Grottoes, Longmen Grottoes, and Maiji Mountain Grottoes, all feature mainly figure-based murals. Very differently, Islam does not worship any created object [4], and most of the mosques across China do not feature murals or other figurative designs on their interior walls. However, few of these mosques feature ornamental paintings depicted plants, geometric patterns, Arabic characters, and even traditional Chinese floral motifs in rare cases [5]. The absence of figurative design in murals aims to prevent excessive worship of such depictions.

The subject of this study are murals of the North Mosque (Figure 1) in Linqing, eastern Shandong province of China. Historical records indicate that it was built during the

Hongzhi Period of the Ming Dynasty (1488–1506 AD), and underwent four renovations [6]. The fourth restoration took place in the 19th year of the Guangxu Reign in 1893. The main hall and the back hall were repaired in 1980 with funding from the Chinese State Ethnic Affairs Commission. At present, the North Mosque is a Key Cultural Relics Site under the State Protection act in China. In 2014, the Grand Canal of China was inscribed on the World Cultural Heritage List, of which the North Mosque is a part [7].



Figure 1. The main gate of the North Mosque in Linqing, China.

The North Mosque features murals that are exclusively of Ming Dynasty main paper murals found in provincial Islamic edifices in China, possessing a long historical provenance [8]. The murals in the North Mosque are slowly deteriorating as a result of environmental factors such as temperature, humidity, and light, as well as human-induced damage, leading to varying degrees of surface deterioration. The murals exhibit various forms of damage, such as pigment layer peeling, nail holes, chalking, and discoloration. Consequently, the preservation and restoration of the murals are necessary. There are detailed records of significant building repairs at the North Mosque. Nevertheless, detailed records of the conservation and restoration of the murals are lacking. The last restoration period of the murals and painting techniques used remains unknown. This requires restoration experts to study the painting materials and painting processes before restoring the murals.

Numerous scientific analysis methods have proven to be excellent in analyzing ancient polychromatic cultural heritages [9]. Ajò David et al. [10] utilized a combination of optical and scanning electron microscopy with energy-dispersive X-ray spectroscopy (SEM-EDS), X-ray diffraction (XRD), Fourier transform infrared spectroscopy (FTIR), and photoluminescence spectroscopies to investigate the composition materials and conservation status of two mural paintings created by Ciro Ferri. For the study of a Persian painting, Mona Abdel-Ghani [11] employed optical microscopy (OM), microscopic Raman spectroscopy (M-Raman), FTIR, and scanning electron microscopy with energy-dispersive X-ray spectroscopy (SEM-EDX). Jennifer Poulin et al. [12] utilized the Direct Inlet potential of pyrolysis–gas chromatography/mass spectrometry (Py-GC-MS) analysis on cultural heritage materials for identification and characterization of polymerized components. The field of cultural heritage conservation in China has made remarkable progress in utilizing various analytical methods, contributing to a deeper understanding and preservation

of cultural relics. Shen Jingyi et al. [13] utilized a digital microscope (DM), SEM-EDS, XRD, Herzberg stain, M-Raman, and FTIR to analyze the polychrome clay sculpture in the Qinglian Temple of Jincheng. He Jing et al. [14] employed techniques such as OM, SEM-EDS, XRD, polarized light microscopy (PLM), FTIR-ATR, thermogravimetric analysis (TG), and mass spectrometry (MS), to investigate the wall paintings at the Samye Temple in Tibet. Furthermore, scholars have conducted a systematic M-Raman analysis on mineral pigments used in the creation of ancient Chinese artworks [15,16].

The primary objective of this study is to examine the composition of the painting materials utilized in the murals of the North Mosque. A combination of multiple analytical techniques was employed to thoroughly investigate the painting materials employed in the North Mosque. To observe the surface information of pigments, PLM and SEM are predominantly utilized. EDS is performed for elemental analysis. In addition, XRD, FTIR, and M-Raman are implemented to examine the composition of pigments. Furthermore, X-ray photoelectron spectroscopy (XPS) is utilized to scrutinize chemical valence of the pigment components. Additionally, Py-GC/MS and FTIR analyses are conducted to detect the probable use of cementing materials in the samples. Based on the pigments employed and the pattern of conventional Chinese painting materials, the possible dating of the mural paintings is discerned. The results of this study can supplement the conservation and restoration information of the murals in the North Mosque and provide a scientific basis for the future conservation and restoration of murals.

2. Materials and Methods

2.1. The Painting

Numerous murals painted during the Ming and Qing Dynasties exist within the North Mosque's worship hall. Local devotees from Linqing incorporated Islamic teachings with elements of traditional Chinese culture to create a unique world brimming with flowers, trees, fruits, and rocks. In the North Mosque hall, a triple-arch wall separated the front hall and the back hall. The murals are primarily located on the wall between the arches, the triple-arch wall, and both sides of the back hall (Figure 2a). Mural composition rules adhere to the basic principles of Islam, featuring plants, mountains, and rocks. Notable examples include peaches, pomegranates, grapes, pines, and vines, as well as Taihu stone patterns and flora. The murals are devoid of any figures or animals. The arch wall murals employ a unique color ink system, combining traditional Chinese ink painting with brush painting techniques. Arabic characters are predominantly painted in blue, green, yellow, and red pigments.

The decorative motifs atop the arches comprise dense, uninterrupted patterns forming an overarching design. The paintings on the top of the arches are mainly entwined branch patterns. The characteristic feature of the entwining pattern is that the flowers, leaves, and vines of the plant are interspersed and overlap throughout the composition. The branches or vines of the plant are used as a skeleton, extending up and down and to the left and right. This forms a continuous, wavy line filling the decorative surface. The twining pattern employs a slender grape-like vine at its core, embellished with red and blue chrysanthemums. The composition of the painting crosses and reorganizes itself in a circular manner. The result is a dense and ornate visual effect that is visually pleasing.

The outline of the arch painting is demarcated in black pigment, with blue and red pigments employed to depict the chrysanthemums, green pigments for the leaves, and white pigments for the branches. Prior to sampling, a portable digital microscope was utilized to assess the murals' preservation status. Unfortunately, the paintings suffered significant pigment loss and nail damage in various spots. The layers of pigment are particularly thin and fit closely to the ground warfare layer. Other fillers and impurities were also present within the pigments, which made identification of the pigments difficult. Samples selected for examination were derived from damaged or concealed regions. On-site, a portable X-ray spectrometer was implemented to analyze the chosen sampling areas for elements, ensuring sample representative sufficiency. Trace amounts of flake samples in

hues such as red, blue, green, black, and white were collected for analytical testing, with sampling information outlined in Table 1.

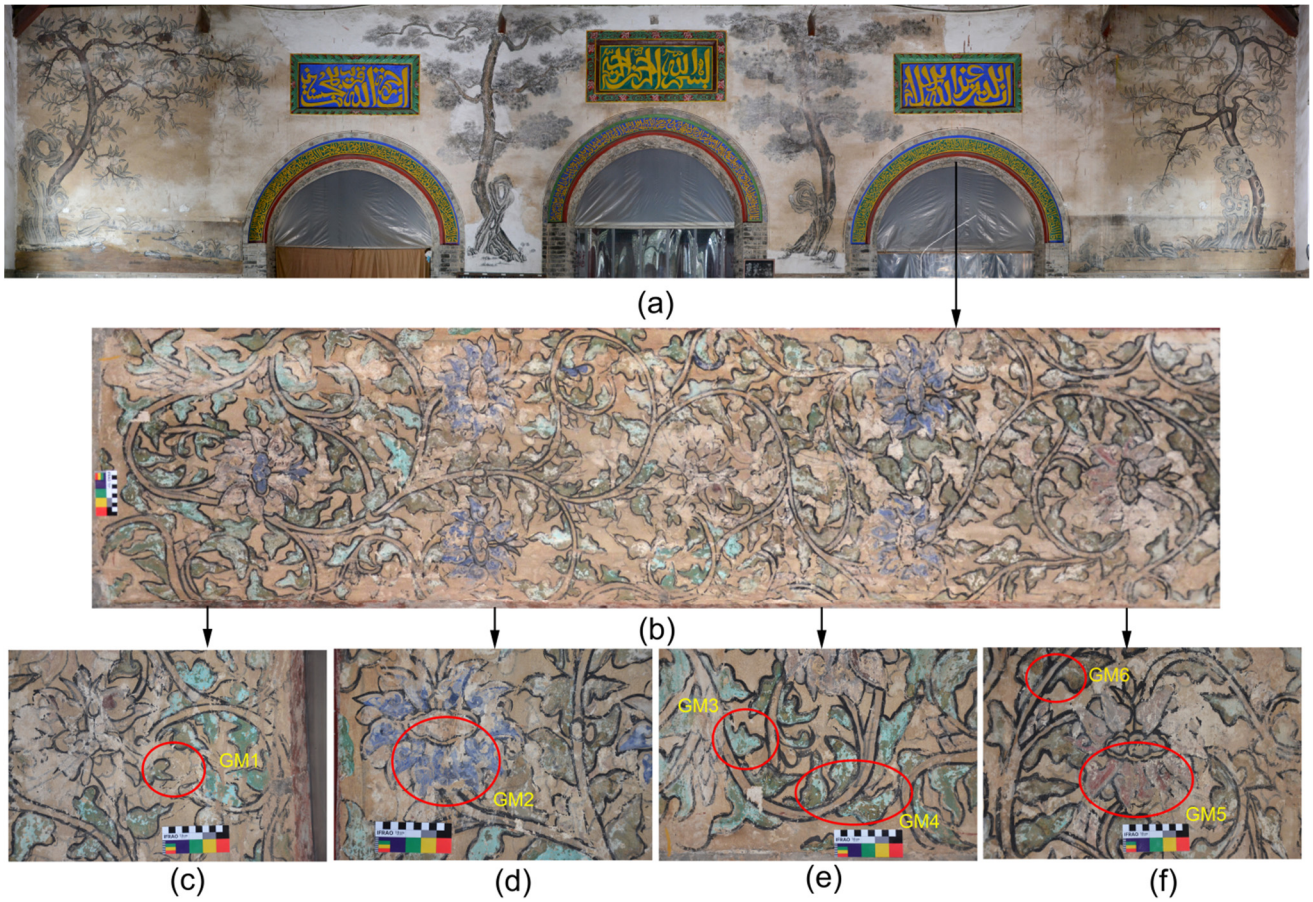


Figure 2. North Mosque murals and sample sampling points: (**a**) East wall mural of the North Mosque Basilica, (**b**) Part of the mural on top of the North Arch, (**c**) White (GM1) sampling point, (**d**) Blue (GM2) sampling point, (**e**) Light green (GM3) and Dark green (GM4) sampling points, and (**f**) Red (GM5) and Black (GM6) sampling points.

Table 1. Sampling details for each arch painting color.

Sample ID	Color	Sample Description	Sampling Locations
GM1	White	Sampled from extensive damaged region Both sides—white	Figure 2c
GM2	Blue	Sampled from petal-damaged region Front—blue; Back—visible white ground layer	Figure 2d
GM3	Light green	Sampled from severely damaged green leaves Front—light green; Back—visible white ground layer	Figure 2e
GM4	Dark green	Sampled from severely damaged green leaves Front—dark green; Back—visible white ground layer	
GM5	Red	Sampled from damaged flower petal area Front—red; Back—visible white ground layer	Figure 2f
GM6	Black	Sampled from an inconspicuous location Front—black; Back—visible white ground layer	Figure 2f

2.2. Analysis Methods

PLM was used to analyze the crystal structure of pigment samples. To determine the origin and formation process of the pigment particles, crystal properties such as size, shape, color, and surface morphology are observed using horizontally and vertically polarized light. The ZEISS Scope A.1 optical microscope with an achromatic polarized light module acquisition lens and 5–50× objective lens is used for this purpose.

The specific test steps are as follows:

- Using a stereomicroscope, remove dust from the surface of the sample with anhydrous alcohol to select pigment particles;
- Wipe the slide with anhydrous alcohol and use a clean tungsten needle to place a small visible amount of sample on the slide (approximately 20–80 ng);
- Disperse the sample by adding drops of anhydrous alcohol to the sample's edge as needed;
- Once the alcohol evaporates completely, use forceps to remove the coverslip onto the sample and place it on a heating table set at 80 °C;
- On the heating table, take a drop of dissolved fixative resin (Meltmount^{TM}, nD = 1.662, Cargille, Cedar Grove, NJ, USA) and place it along one side of the coverslip until the resin has completely penetrated the coverslip;
- After the sample has cooled, observe it under the polarizing microscope. The polarizer insertion method was utilized to determine the crystal's refractive index in relation to 1.662. When nD < 1.662, the polarizer insertion demonstrated a deepening of the crystal edge in the same direction. Conversely, when nD > 1.662, the polarizer insertion revealed a deepening of the crystal edge in the opposite direction.

The SEM was chosen to examine the microscopic morphology of pigments, with a large depth of field, a wide field of view and a three-dimensional image. It also enables direct observation of particles with uneven surfaces, allowing analysis of their crystalline morphology. The EVO MA25 from ZEISS, Germany, was used as the scanning electron microscope. The sample was prepared by gluing the pigment particles to a conductive adhesive. This was followed by gold spraying. Finally, the sample stage was placed in the sample bin, vacuumed, and examined. SEM-BSE images of the pigment particles were recorded for analysis.

To determine the relative elemental content of pigment samples, an EDS was selected. The instrument was the Oxford Instruments OXFORD X-MAX20 EDS system with the SEM attachment. This system is capable of testing elements from 4 Be-92 U. In the analysis, an area of approximately 10 μm × 10 μm was scanned, and the total analysis time was 60 s.

The chemical composition of pigment samples was analyzed using M-Raman and FTIR. The inVia Reflex type instrument from Renishaw, UK, is utilized as the M-Raman. The instrument has a scanning range of 100–4000 cm^{-1}, and a 532 nm laser wavelength was used for red, blue, and black pigments, and a 785 nm laser wavelength was used for detecting green and white pigments. The exposure time was set to 30–60 s. The FTIR used for this study was a Thermo Fisher Nicolet iN10 from the USA, equipped with an mCT/A detector. The detection range was set to 4000–650 cm^{-1}, with 32 scans and a resolution of 4 cm^{-1}. Samples were ground, dispersed and placed on BaF_2 carrier sheets for detection.

XRD was chosen to detect the composition and crystallinity of pigment samples and inorganic fillers. Based on the position and intensity of the peaks on the diffraction spectrum, the crystalline phase of the mineral and the corresponding crystal structure can be determined. The Smart Lab 9 kW instrument from Rigaku, Japan, was utilized as the XRD. The instrument is equipped with Cu Kα radiation (k = 1.54059 Å) and a D/tex Ultra detector. In PB mode, the operating voltage was set at 45 kV, the current at 20 mA, and the scanning speed at 15°/min. The scanning range was set from 2 to 10°. The sample was ground to a powder size not exceeding 200 mesh in an agate mortar and detected on the flattened surface of a single crystal silicon wafer. The diffraction peak attribution was performed using the ICDD-PDF-2-2012 commercial spectral library.

XPS was chosen to determine the valence state of pigment elements, providing valuable insight into their chemical composition. The experiment was conducted using a

monochromatic Al Kα target with an energy of E = 1486.68 eV. The voltage was set to 14,795.40 V, with a current of 0.0108 A. The vacuum was maintained at $p < 10^{-9}$ mbar, and the pass energy was set to 100 eV (survey) and 20 eV (high-resolutions). The work function was set to 5.04 eV.

The Py-GC/MS and FTIR analyses were chosen to detect the possible use of cementitious materials in the samples. Py-GC/MS was used for the experiment, which combined the pyrolyzer EGA/PY-3030D from Frontier Laboratories, Koriyama, Japan with the Shimadzu GCMS-QP2010Ultra Gas Chromatography Mass Spectrometer. The thermal lysis temperature was set to 600 °C, with a thermal lysis time of 10 s, and the syringe temperature was set to 250 °C. The connection interface between the syringe and chromatograph was set to 320 °C. The experimental procedure involved adding 50 µg of mortar to the thermal cracker and 3 µL of 20% tetramethylammonium hydroxide (TMAH). After standing for 30 min, the sample was placed in the autosampler and pyrolyzed at 600 °C. After pyrolysis, the product was identified using GC-MS.

3. Results

3.1. White

The sample GM1 was analyzed using EDS, which revealed that the main elements present were O, Si, C, and Al (Figure 3d). Unfortunately, due to insufficient sample content and other factors, the M-Raman test of the GM1 sample did not result in an analyzable pattern. The samples were analyzed using FTIR spectroscopy. The FTIR spectra (Figure 3f) showed significant bands at 3694, 3651, 3618, 1116, 1036, 1007, 940, 913, 796, and 753 cm^{-1}. These bands were confirmed to be characteristic absorption bands of kaolinite [17]. The bands at 3694, 3618, and 3651 cm^{-1} were the stretching vibration absorption peaks of the hydroxyl (–OH) groups. The bands at 1116, 1036, and 1007 cm^{-1} belonged to the absorption peaks of the stretching vibration of Si–O. The bands at 940 and 913 cm^{-1} were attributed to the Al–OH stretching vibration and Al–OH bending vibration absorption peaks, respectively. The bands at 796 and 753 cm^{-1} were attributed to Si–O–Si symmetric stretching absorption bands. The bands at 3528, 3396, 1681, and 1619 cm^{-1} confirmed the characteristic absorption bands of gypsum [18]. The presence of hydrogen bonds H–O. . .H between H_2O molecules, and the large molecular clusters and the telescopic vibrations of the crystalline water led to the appearance of the 3528 and 3396 cm^{-1} bands. In contrast, the variable angle vibrations of the water of crystallization appeared as sharp absorption bands around 1681 and 1619 cm^{-1} [19]. Gypsum showed an antisymmetric absorption peak for SO_4^{2-} near 1135 cm^{-1} [20]. It is noteworthy that this peak completely coincided with the broad peak of kaolinite in the region of 1220 to 800 cm^{-1}. The bands at 1324 and 1372 cm^{-1} were attributed to the O–C=O stretching vibration absorption bands of oxalates [21]. The XRD results showed that the sample contained gypsum, kaolinite, and quartz (Figure 3e). The narrow and sharp bands in the XRD spectra further confirmed the good crystallinity of both gypsum and kaolinite.

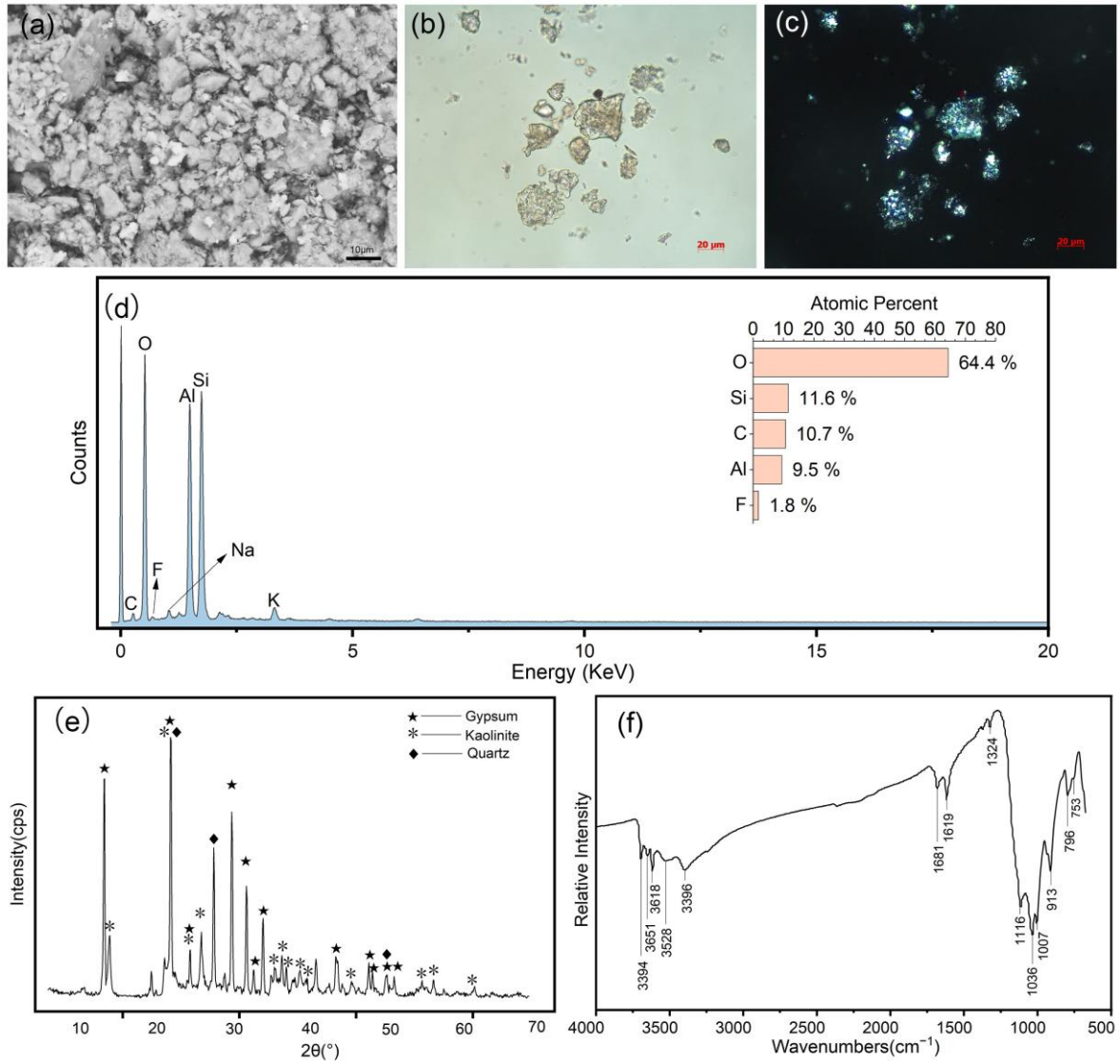


Figure 3. Microscopic images and analysis spectra of the GM1 sample: (**a**) Scanning electron microscopy-X-ray energy spectrometer (SEM-BSE) micrograph at ×1000 magnification, (**b**) Polarized light microscopy image at ×500 magnification, (**c**) Orthogonal polarized microscopy image at ×500 magnification, (**d**) Elemental semi-quantitative analysis and molecular content spectra, (**e**) X-ray diffraction (XRD) analysis spectra, and (**f**) Fourier transform infrared spectroscopy (FTIR) analysis spectra.

In single polarized light, the pigment particles were non-uniform in size and appeared transparent (Figure 3b). These particles showed a wide distribution, spanning from around 15 μm to up to 35 μm in diameter with non-smooth edges, rough surface, and uneven appearance. Under orthogonal polarization (Figure 3c), it showed a non-extinction phenomenon, and the refractive index was less than 1.662. The SEM-BSE imaging illustrated a mixture of flake and granular structures in the microstructure of the pigment particles (Figure 3a). The particles had an irregular shape and a non-uniform size distribution, with boundaries that were less clearly defined.

Based on a comprehensive analysis, gypsum and kaolinite are the main components of white pigments. There are many mineral pigments that can be used as white pigments in China. White pigments can also be mixed with other colors to obtain different shades of pigment. Gypsum and kaolinite were commonly used as white pigments in ancient China. In addition to their use as pigments in ancient Chinese wall paintings, they were also

commonly used to form the ground battle layer of wall paintings. Gypsum was often used to prepare calcium-sulfate-based grounds for painting carriers in anticipation of a better display of other colored pigments. The presence of oxalate minerals in the samples provides evidence for the existence of lower organisms like fungi [22], which either naturally exist in artifacts or could be generated via microbial metabolism and degradation processes. This supports the notion that the murals were painted during a certain period of time in the past, prior to the present. Nevertheless, based on the findings of the current analysis, it remains unfeasible to ascertain the precise painting date.

3.2. Blue

The EDS analysis revealed that sample GM2 is composed primarily of O, C, Si, Na, S, and Al (Figure 4b). The FTIR spectra (Figure 4d) exhibited significant bands at 3397, 3235, 1620, 1037, and 794 cm^{-1}. The bands at 3397, 3235, and 1620 cm^{-1} indicated the presence of gypsum. The broad peaks observed near 3528 and 3396 cm^{-1} corresponded to the stretching vibration of crystalline water within the gypsum, while the 1620 cm^{-1} peak represented the variable angle vibration of crystalline water. The SO_4^{2-} antisymmetric absorption peak of gypsum likely coincided with the broad peak observed at 1037 cm^{-1}. The bands at 1424 and 1320 cm^{-1} indicated the presence of oxalates. The band at 1037 cm^{-1} was the stretching vibration absorption peak of Si–O in silicate, which was attributed to the Si–O–Si symmetric stretching absorption peak at 794 cm^{-1}. The determination of ultramarine could not be ascertained through FTIR analysis. The bands at 1037 and 794 cm^{-1} might be the characteristic bands of ultramarine [23], yet they could correspond to the characteristic bands of other silicates as well. The XRD analysis of the sample (Figure 4c) revealed the presence of gypsum, kaolinite, and quartz. The standard diffraction peaks of synthetic ultramarine were at 12.2°, 13.7°, 24.0°, 31.1°, 34.3°, 42.3°, 51.5°, 56.5°, 57.7°, 61.6°, 63.3°, and 68.9° [24,25]. However, upon analyzing the XRD pattern of sample GM2, most of the diffraction peaks of ultramarine were found to overlap with other substances, making it impossible to confirm its presence. In addition, this analysis revealed the presence of sulfur potassium sodalite palmierite ($(Na,K)_2Pb(SO_4)_2$), the exact reason for which remained inconclusive.

The M-Raman was used to analyze the sample, with strong spectral signals (Figure 4a) observed at 259, 547, 1096, and 1645 cm^{-1}. The band at 259 cm^{-1} corresponded to the ν_2 bending vibration of the S_3^- ion, while the intense band at 549 cm^{-1} was attributed to the ν_1 symmetric stretching vibration of the S_3^- ion [26,27]. Notably, the presence of calcite distinguished lapis lazuli from synthetic ultramarine, with the former exhibiting absorption bands at 1086, 713, 283, and 156 cm^{-1} in the Raman spectrum [28]. However, the absence of these characteristic bands in sample GM2 suggested that the blue pigment is most likely synthetic ultramarine.

Observation under single polarized light revealed a non-uniform particle size distribution of the ultramarine pigment, with particle diameters ranging from 7 to 20 μm (Figure 5a). The largest particles, around 20 μm in diameter, were formed by aggregation of many small particles, resulting in an inky blue appearance due to lack of light penetration. Uniform hue and blue appearance were found in dispersed pigment particles. The small particles showed rounded crystals with smooth edges, indicating a synthetic pigment. SEM-BSE imaging (Figure 5b) shows that the microstructure of the pigment exhibited uniform size with obvious boundaries and smooth edges without sharp features. The distribution maps of Na, Al, and Si (Figure 5c–e) indicated a general distribution of ultramarine particles, with S and O elements (Figure 5f,g) being more widely distributed. The possible reason for this result is that there are other substances mixed in the sample.

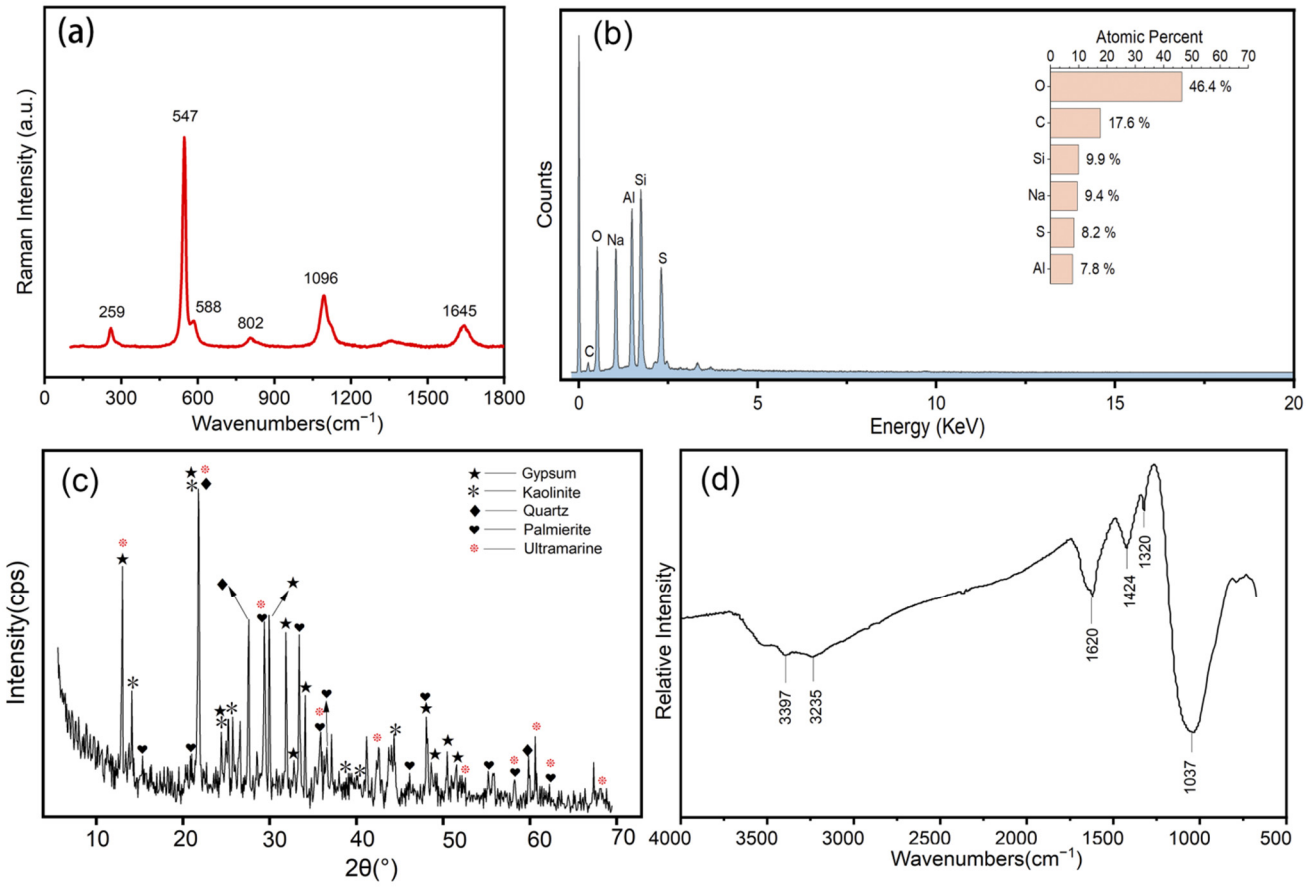


Figure 4. Analysis spectra of the GM2 sample: (**a**) Microscopic Raman spectroscopy (M-Raman) spectra, (**b**) Elemental semi-quantitative analysis and molecular content spectra, (**c**) XRD analysis spectra, and (**d**) FTIR analysis spectra.

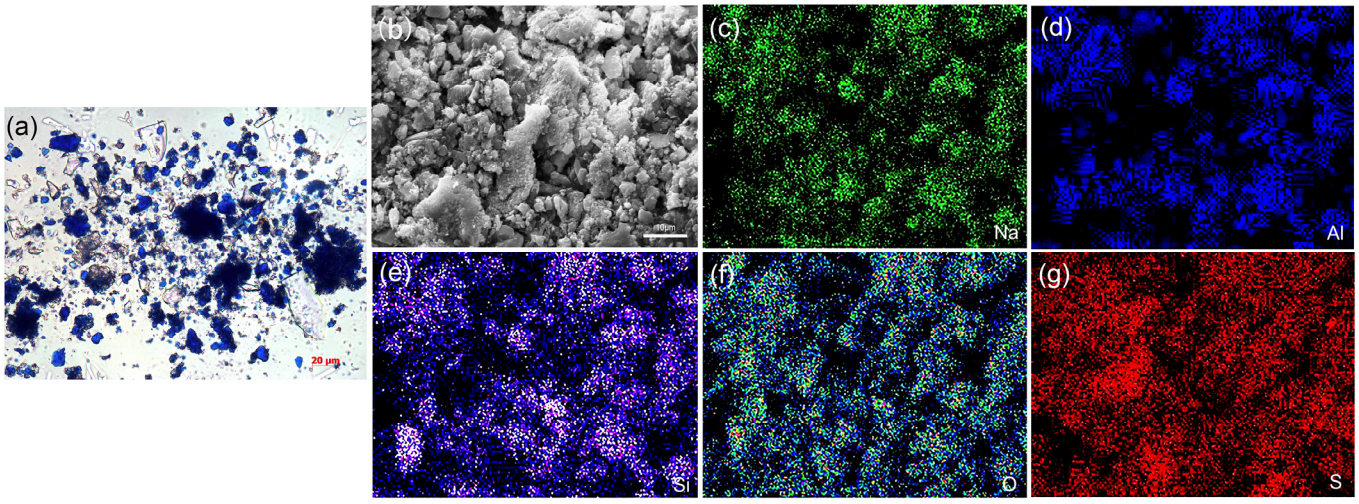


Figure 5. Microscopic images of the GM2 sample: (**a**) Polarized light microscopy image of blue pigment at ×500 magnification, (**b**) SEM-BSE micrograph at ×1500 magnification, and elemental analysis maps of (**c**) Na, (**d**) Al, (**e**) Si, (**f**) O, and (**g**) S distribution.

Ultramarine, an inorganic pigment, was first synthesized by Jean Baptiste Guimet in 1828 [29]. Synthetic ultramarine is primarily derived from kaolin, sodium carbonate, and sulfuric acid. A complex sodium aluminum sulfosilicate, synthetic ultramarine exhibits high stability and presents as a bright blue powder. In the late Qing Dynasty, European

synthetic ultramarine was imported into China, where its low cost and abundance in the market made it immediately popular, particularly for painting art, including the restoration of murals [30]. Examples of its use include the royal Taoist temple beside the Forbidden City in Beijing [31], the Avalokitesvara Statues in Dazu County in Chongqing [32], and the Du Le Temple of the Liao Dynasty in Tianjin [33].

3.3. Green

The green pigment is the most difficult pigment to characterize. Analysis of sample photos revealed two distinct varieties of green pigment, identified as light green (GM3) and dark green (GM4). The light green is covered by the dark green, and the dark green layer comes off to expose the underlying light green. The light green pigment should be a mixture of green pigment and white pigment. The pigment layer is very thin, which leads to a very large number of impurities mixed in the sample. Consequently, despite multiple attempts at Raman detection, to obtain a valid spectrum was unsuccessful, resulting in the difficulty of analyzing the green pigment.

Elemental analysis of samples GM3 and GM4 using the EDS revealed the prominent presence of O, C, Cu, As, Na, Cl, and Pb elements (Figure 6b). There was a notably higher concentration of Cu and As elements, indicating the pigments to be Cu-As-based. The XRD pattern of the samples (Figure 6c) exhibited characteristic peaks of gypsum, kaolinite, and quartz, in addition to the 10.5°, 29.2°, and 33.4° peaks that corresponded to the standard 2θ data of copper arsenite [34]. The presence of these peaks suggested that the samples possibly contained emerald green pigment.

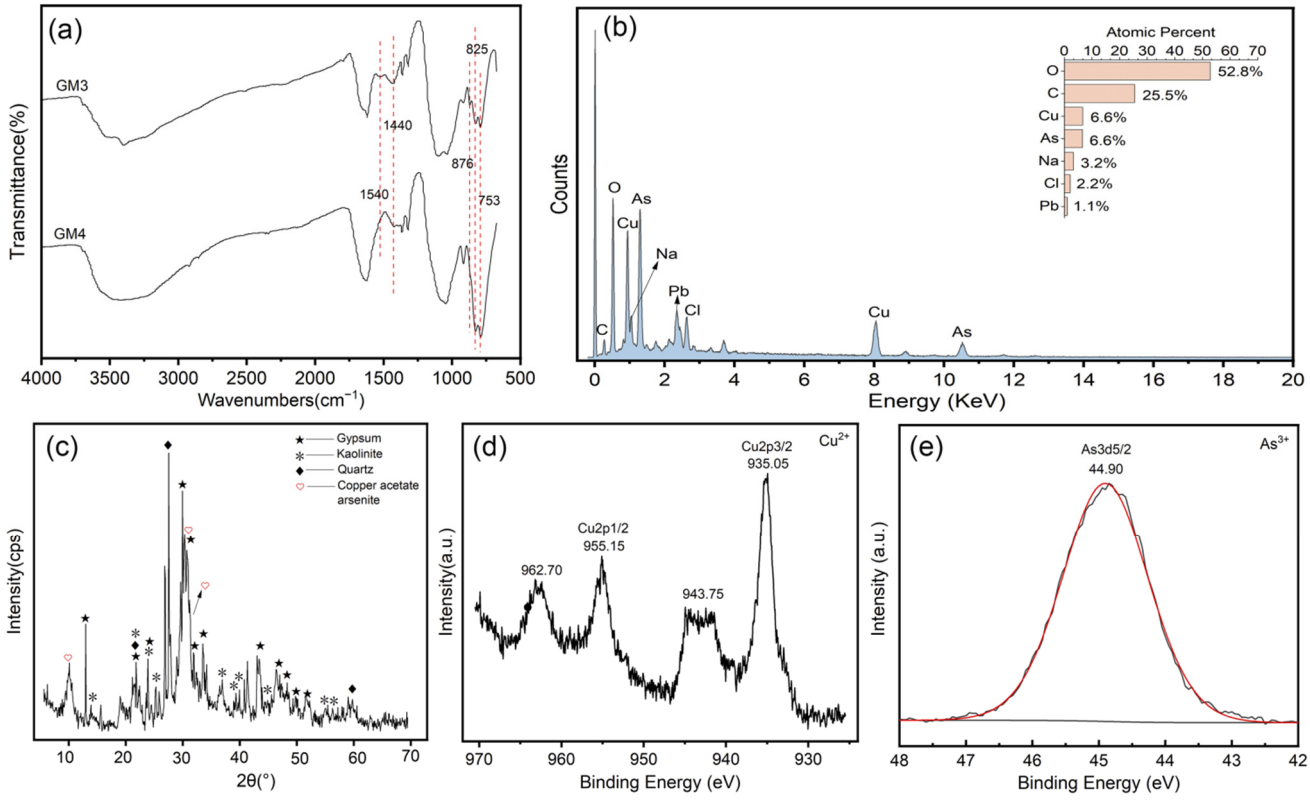


Figure 6. Analysis spectra of GM3 and GM4 samples: (**a**) Comparative infrared spectra of GM3 and GM4, (**b**) Elemental semi-quantitative analysis and molecular content spectra of GM4, (**c**) XRD analysis spectra of GM4, (**d**) Cu element X-ray photoelectron spectroscopy (XPS) analysis spectra of GM4, and (**e**) As element XPS analysis spectra of GM4.

The FTIR spectrum of GM3 was found to exhibit absorption bands at 3543, 3398, 1620, 1540, 1440, 1362, 1320, 1098, 1030, 917, 876, 825, and 793 cm^{-1}, indicating a complex mixture

of substances (Figure 6a). Specifically, the bands at 3543, 3398, and 1620 cm^{-1} corresponded to the characteristic absorption bands of gypsum. The 1362 and 1320 cm^{-1} bands were attributed to O–C=O stretching vibration absorption bands of oxalates. While 1098 and 1037 cm^{-1} bands indicated Si–O stretching vibration absorption peaks in silicates, with an unknown silicate compound contributing to that band. Furthermore, the broad band also comprised the SO_4^{2-} antisymmetric stretching absorption band of gypsum. Emerald green typically exhibits strong absorption bands at 1556, 1452, 820, 774, and 650 cm^{-1}, based on the standard FTIR spectrum [35]. In comparison, the GM3 sample spectrum showed a weakened intensity of the absorption bands at 1540 and 1440 cm^{-1}, and similar band shapes of the absorption bands at 825 and 793 cm^{-1}. This phenomenon could be attributed to the aging of emerald green pigment, which resulted in the change in certain chemical bonds. Based on the FTIR analysis, the green pigment additionally exhibited characteristics consistent with those of emerald green pigment. The FTIR bands of GM3 and GM4 were found to be quite similar, with both containing. gypsum, oxalate, and silicate species for color mixing. However, a comparison of the FTIR showed that the band intensity near 1030 cm^{-1} corresponded to the inorganic filler in GM3, which was notably higher than the peak at 825 cm^{-1} that corresponded to emerald green. Conversely, the FTIR of GM4 revealed an opposite pattern. This also indicates that gypsum and silicate type substances were used for color mixing.

To confirm the presence of emerald green in the sample, XPS was conducted. As shown in Figure 6d, the Cu2p3/2 photoelectron peak had a binding energy of 934.35 eV, which was close to the binding energy of Cu3/2 in $Cu(CH_3COO)_2$ (935.0 eV). The binding energy of Cu2p1/2 photoelectron peak was 955.15 eV. Two companion peaks also existed with binding energies of 943.75 eV and 962.70 eV for the main peak. These results indicates the presence of Cu in a +2 valence form in the green pigment sample [36]. Additionally, Figure 6e demonstrated that the photoelectron peak binding energy of As3d5/2 was for this element. As was 44.9 eV, indicating its existence in a 3+ valence form, primarily as arsenite. The chemical formula of emerald green is $(Cu(CH_3COO)_2 \cdot 3Cu(AsO_2)_2)$, and a comprehensive analysis of the test results inferred the existence of emerald green in the green pigment sample.

Under single polarized light (Figure 7b), the pigment particles exhibited a darker center and brighter edges. The bright green particles showed a round or fan-shaped morphology, with clearly defined edges and a daisy-like appearance. The pigment particles had a relatively homogeneous size distribution, and multiple particles could be seen. The circular particles had a diameter ranging from approximately 5–18 μm, with the majority measuring at a diameter of 13 μm. Additionally, these particles possessed a refractive index greater than 1.662. Under orthogonal polarization (Figure 7c), the larger particles displayed specific characteristics, with a brighter center and darker periphery, and showed no extinction phenomenon. The PLM micrographs of emerald green also illustrated these features, confirming the green pigment as emerald green [35]. Other substances, likely kaolinite and quartz particles, were also detected in the PLM micrographs. In SEM-BSE (Figure 7d), the microstructure of the pigment particles appeared spherical with some interspersed particles. The size distribution of the spherical particles was relatively uniform, with distinct boundaries. In Figure 7a, several spheres appeared broken from the middle in a daisy-like image, and a sphere with a crack was also visible. These results imply that the emerald green pellets have undergone poor preservation and aging. The distribution maps of Cu and As (Figure 7e,f) showed that the spatial distribution of Cu and As elements corresponded well to the elemental distribution properties of emerald green.

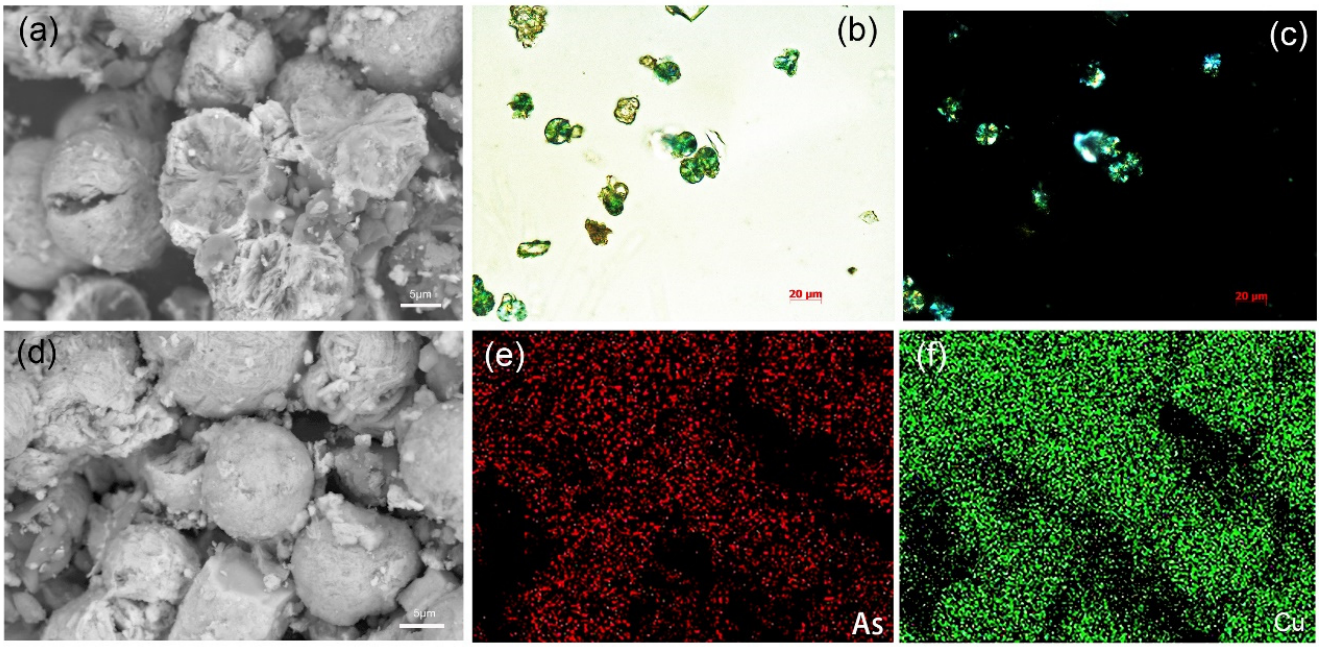


Figure 7. Microscopic images of the GM4 sample: (**a**) SEM-BSE micrograph at ×2000 magnification, (**b**) Polarized light microscopy image at ×500 magnification, (**c**) Orthogonal polarized microscopy image at ×500 magnification, (**d**) SEM-BSE micrograph at ×2000 magnification, and elemental analysis maps of (**e**) As and (**f**) Cu distribution.

Emerald green ($Cu(CH_3COO)_2 \cdot 3Cu(AsO_2)_2$) is a synthetic compound of arsenic and copper that was invented and utilized extensively in Europe during the early to mid-19th century [37]. Emerald Green was introduced to China during the mid-19th century [38]. The use of this pigment was discontinued in Western countries between the late 20th and early 21st centuries [39]. In air, it is stable to light and heat, but unstable to acids and bases. Emerald green has a strong color, strong covering ability, and is inexpensive compared to the mineral pigments chloro-copperite and stone green [40]. In China, emerald green was widely used in the repainting of ancient murals during the late Qing Dynasty [41]. Until the late Qing Dynasty, traditional Chinese color painting utilized mainly natural mineral pigments sourced from China. It was only during this period that synthetic pigments such as synthetic ultramarine and emerald green were introduced from abroad and adopted by Chinese painters. This broke the tradition of Chinese color painting in terms of pigment use and changed the way pigments were used in the past, while providing artists with more color choices and ways to create. However, due to its toxicity, emerald green is no longer used as a pigment in China nowadays.

3.4. Red

The analysis by EDS (Figure 8e) determined that the main components of GM5 were Hg and S. Further examination via M-Raman spectroscopy (Figure 8d) revealed characteristic peaks at 254, 281, and 342 cm^{-1}, which were identified as the stretching vibrations of Hg–S [42,43]. Additionally, the XRD spectra (Figure 8f) provided further evidence that the pigment composition was cinnabar. Since there was no signal of Hg–S bond in the mid-infrared range, the FTIR results (Figure 8g) only detected characteristic absorption peaks of gypsum, kaolinite and oxalate.

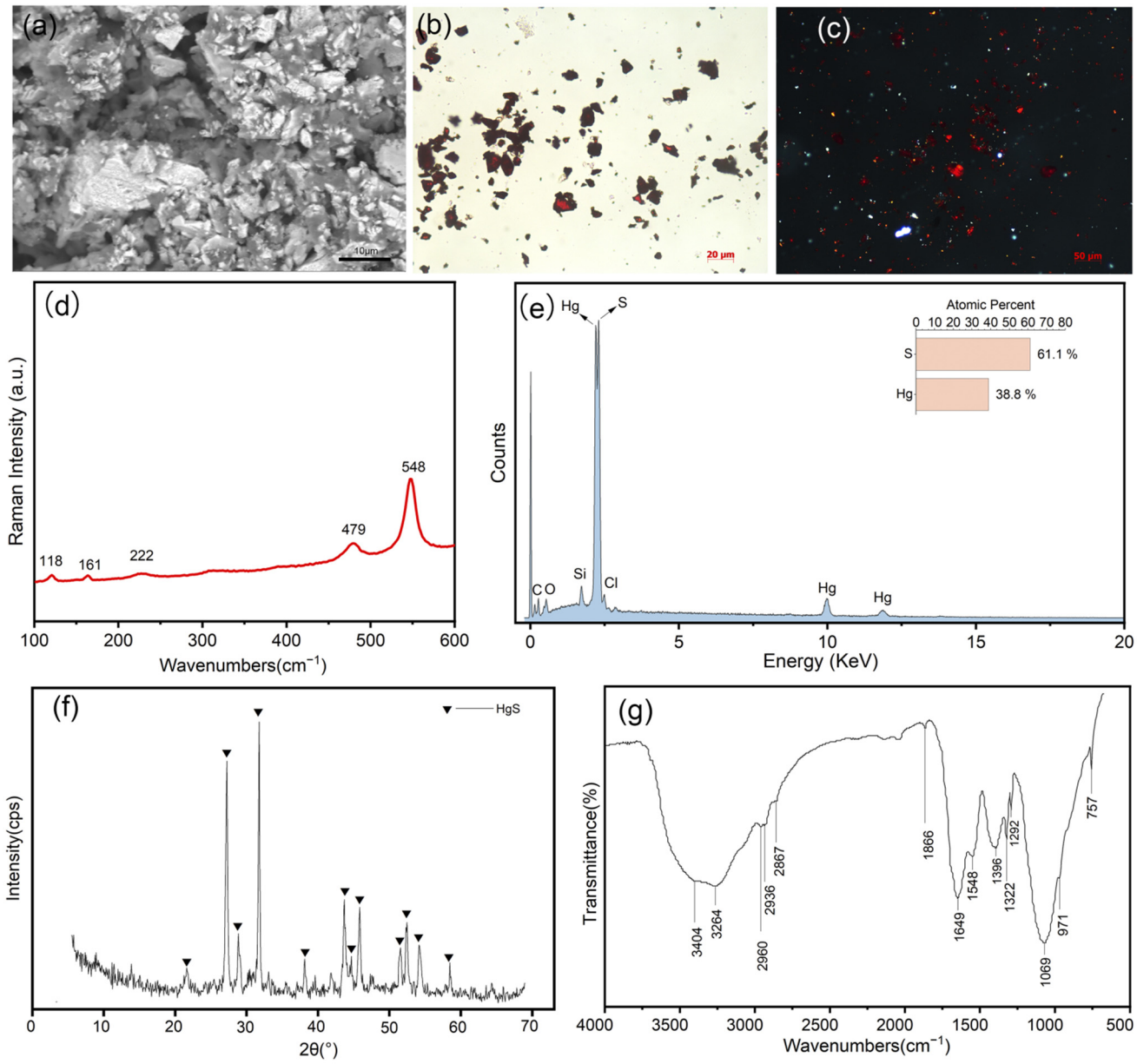


Figure 8. Microscopic images and analysis spectra of the GM5 sample: (**a**) SEM-BSE micrograph at ×1500 magnification, (**b**) Polarized light microscopy image at ×500 magnification, (**c**) Orthogonal polarized microscopy image at ×200 magnification, (**d**) Raman spectra, (**e**) Elemental semi-quantitative analysis and molecular content spectra (percentage after ignoring other elements), (**f**) XRD analysis spectra, and (**g**) FTIR analysis spectra.

Under single polarized light (Figure 8b), cinnabar pigment displayed elongated and fragmented rock-like structures. The larger grains exhibited a dark red coloration, while the smaller grains appear black in color. Upon orthogonally polarizing the light (Figure 8c), the larger grains continued to appear dark red, with some displaying an orange tinge. Similarly, the smaller particles exhibited a red coloration and also demonstrate orange tinges. The measured diameter range of the pigment particles was approximately from 2–30 μm, with the larger particles typically displaying a diameter of around 25 μm and a higher frequency at 10 μm. Additionally, the larger pigment particles exhibited a quadruple extinction phenomenon and had a refractive index greater than 1.662. SEM-BSE micrograph analysis (Figure 8a) also indicated that the particle size of the pigment was non-uniform with clearly visible small particles exhibiting distinct angles and sharp edges.

Cinnabar, chemically represented by mercury sulfide (HgS), is a vivid red pigment that displays remarkably pure coloration and stable properties that prevent significant discoloration. In ancient China, cinnabar and lead pellets represented the commonly utilized red pigments [44]. Scholars have studied Neolithic sites [45], primarily from the Dadiwan and Yangshao cultures, through the analysis of surface pigments on excavated painted pottery. The results illustrated that the red pigments were commonly derived from hematite and cinnabar. Based on C^{14} dating, the earliest extant example of the use of cinnabar in China dates back approximately 7400–7800 years ago. Cinnabar continues to be utilized for pigment in China nowadays.

3.5. Black

As determined by EDS (Figure 9e), the main elements of the black pigment in GM6 were C, O, N, S, and Cl. The atomic percentage of element C accounted for 79.9%. It is worth noting that the presence of element N in GM6 could be attributed to the binder used to formulate the pigment. The XRD pattern (Figure 9f) revealed that the dominant phase compositions in GM6 were gypsum, quartz, kaolinite, and sulphur potassium sodalite palmierite ($(Na,K)_2Pb(SO_4)_2$. Similarly, the FTIR pattern (Figure 9g) showed distinct absorption peaks of inorganic fillers and impurities including gypsum, silicate, and oxalate. The M-Raman spectrum of the black pigments (Figure 9d) displayed broad absorption peaks at 1320 and 1592 cm^{-1}, which coincided with those of carbon black (C)'s D and G peaks, respectively [46]. Carbon black is typically generated from the incomplete combustion of wood and bone. Nevertheless, the absence of a distinctive band at 960 cm^{-1} in the Raman spectrum of GM6 implied that the stated carbon black was formed from wood combustion rather than the combustion of organic bone [47].

Under single polarized light (Figure 9b), the carbon black particles exhibited larger particle size with no distinct edges, displaying irregular shapes. Transparent particles were observed underneath the black pigment, which could be white particles under the pigment. Measured particle diameters of the pigment ranged from 15–80 μm, with smaller particles likely stemming from carrier breakage. Orthogonal polarization resulted in full extinction (Figure 9c). Due to the low content of black pigment, a small sample was directly glued onto the conductive adhesive for SEM examination. The field of view of the SEM revealed that the large area was entirely the ground battle layer, with black pigment particles sporadically distributed on the surface layer. SEM-BSE micrographs (Figure 9a) indicated the black pigment particles to be large and irregularly shaped.

Carbon black pigment is widely used as a black pigment in China [48]. It is a crucial component of ink in traditional Chinese painting, consisting mainly of carbon black. In architectural murals, carbon black is also commonly employed.

3.6. Binder

FTIR analysis was conducted to determine the presence of binder in the samples. However, the samples exhibited low-to-negligible levels of significant binder. Possible explanations for this result include the limited presence of binder in the pigment or the degradation of chemical bonds due to extended binder aging in the natural environment. In particular, protein-based adhesive materials was only detected in sample GM5, displaying low IR absorption bands at 2960, 2936, 2867, 1649, and 1548 cm^{-1}, as presented in Figure 8g. The bands at 2960, 2936, and 2867 cm^{-1} correspond to vibrational absorption bands of C–H, while the bands at 1649 and 1548 cm^{-1} correspond to characteristic absorption bands for the amide group ($–CONH_2$). During the EDS examination of sample GM6 (Figure 9e), the atomic percentage of 7% N element was found on one pigment particle. All of this information indicates that the binder material used in the mural might be protein-based adhesive materials.

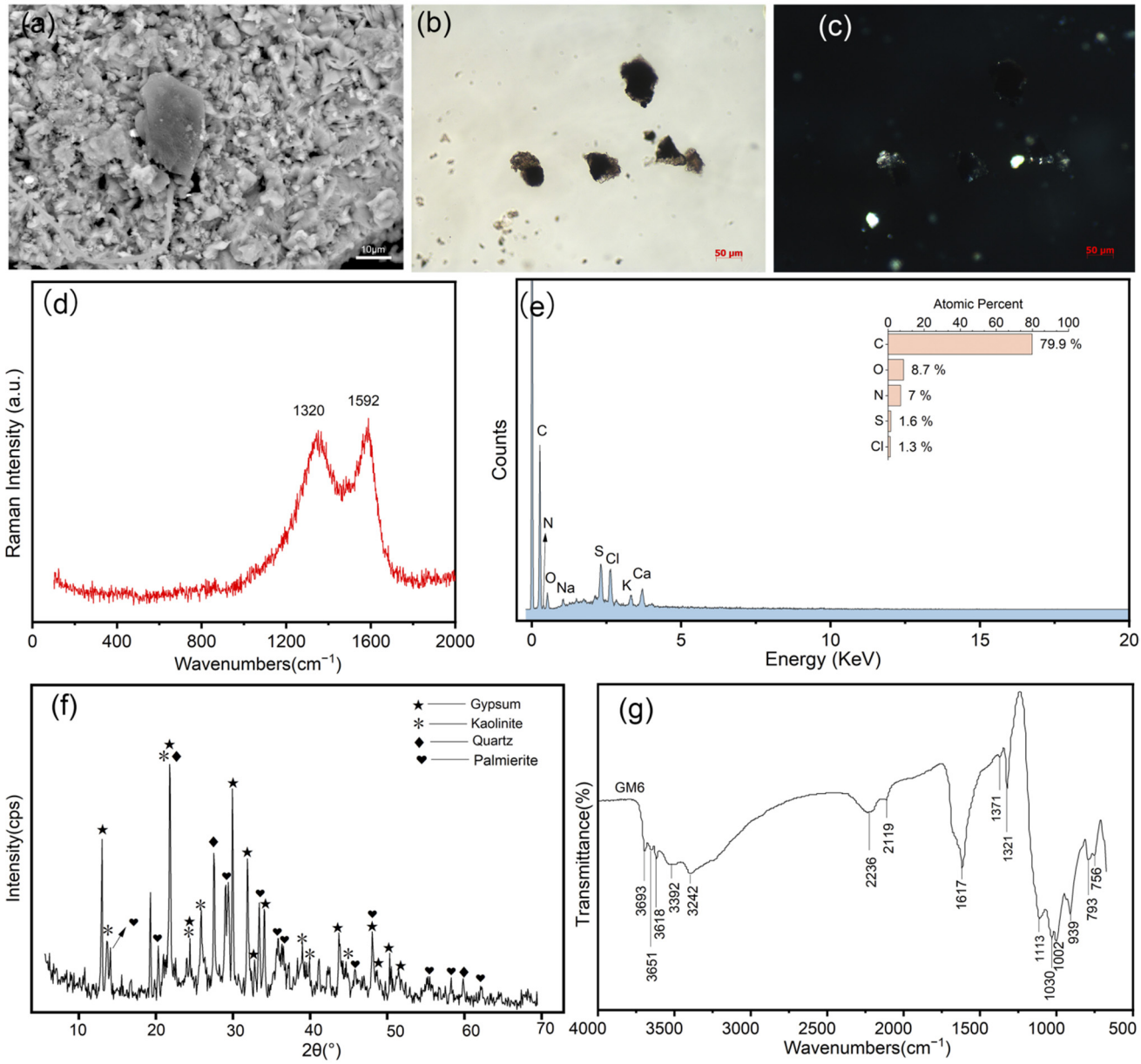


Figure 9. Microscopic images and analysis spectra of the GM6 sample: (**a**) SEM-BSE micrograph at ×1000 magnification, (**b**) Polarized light microscopy image at ×200 magnification, (**c**) Orthogonal polarized microscopy image at ×200 magnification, (**d**) Raman spectra, (**e**) Elemental semi-quantitative analysis and molecular content spectra, (**f**) XRD analysis spectra, and (**g**) FTIR analysis spectra.

The Py-GC/MS can quickly screen out the binder materials in ancient color paintings, including animal glue, egg yolk, and linseed oil, by detecting their degradation or aging products [49,50]. Wang Na et al. [51] identified different materials based on the relative contents of pyrrole, nitrile, proline, and indole, which can be used to identify pig blood, animal glue, egg white etc. Further analysis was carried out using Py-GC/MS, and the results are shown in Table 2. The sample was found to contain methyl pyrrole (#1) with a peak area of 7.55%. The presence of protein-like material was tentatively proved by the detection of pyrrole-like material [51]. The combined results of Py-GC/MS, FTIR, and EDS inferred that the binder material in the sample might be protein-based adhesive materials. In the painting of traditional Chinese murals, animal gum, pig blood, and egg white are commonly used as binder materials, among which animal glue is the most extensively utilized. However, it remains challenging to definitively ascertain the specific protein

upon which the adhesive is founded, as elucidated in the analytical findings. Further investigation of additional samples or incorporation of alternative analytical techniques is imperative for confirmation.

Table 2. Results of THM-Py-GC/MS analysis of sample GM5.

Number	Retention Time (min)	Peak Area (%)	Compound
1	2.38	7.55	1-Methyl-1H-pyrrole
2	2.47	3.35	Toluene
3	2.76	27.13	Methylation reagent derivatives
4	11.43	28.92	Methyl palmitate
5	12.68	33.05	Methyl stearate

4. Discussion

One common characteristic observed in artifact samples is their composition as mixtures, which include pigments, ground warfare layers, contaminants, among others. Furthermore, artifact samples often exhibit aging phenomena, such as degradation of physical properties and breakage of chemical bonds. These factors pose challenges for the detection and analysis of artifact samples. Each detection technique has different principles, detection limits, and focal points, making it necessary to employ a combination of multiple analytical tools. For instance, EDS was utilized to detect the elemental composition of the sample, which was fundamental for substance identification. M-Raman demonstrated excellent performance in analyzing blue, red, and black pigments, but did not yield useful information about white and green pigments. FTIR detection confirmed the presence of ground warfare layers in each color sample and unexpectedly discovered residual adhesive components. However, FTIR struggled to distinguish between ultramarine and silicate, and did not provide valid information for black and red pigments. In the analysis of green pigments, it was observed that emerald green had undergone severe aging and had lost some of its physical and chemical properties. M-Raman and XRD showed limited efficacy in analyzing the samples, and FTIR only offered information regarding specific functional group peaks. However, microscopic morphology tests conducted by PLM and SEM revealed that emerald green still retained its characteristic microscopic morphology. The green pigment was then confirmed to be emerald green based on XPS detection of the valence states of Cu and As elements to determine their chemical properties. Py-GC/MS exhibited excellent performance in detecting the presence of trace organic matter in the samples. To gain a more comprehensive understanding of artifact samples, it is advantageous to employ a combination of multiple analytical methods.

This study employed a combination of several analytical techniques to investigate the painting materials in the the North Mosque, located in Linqing City, Shandong Province, China. The results revealed that the mural paintings primarily employed ultramarine, emerald green, cinnabar, kaolinite, gypsum, and carbon black pigments, while the gum binder used was protein-based adhesive materials. The similarity between the pigments and painting materials utilized in the mural paintings of the North Mosque and other architectural paintings in China could provide insights for the conservation and restoration efforts of these artwork and aid in the development of more effective conservation strategies.

The cinnabar, carbon black, kaolinite, gypsum, and other pigments employed in the North Mosque murals were commonly used in ancient China. Meanwhile, the blue and green pigments in the North Mosque murals were identified as synthetic ultramarine and emerald green, respectively. Meanwhile, ultramarine and emerald green were introduced to China during the late Qing Dynasty, due to their first synthesis in 1828 and 1814, respectively. As such, it can be inferred that the restoration of the murals dates back no earlier than the late Qing dynasty. The results presented in this study help address the lack of available historical restoration information. However, due to the limited scope of this

study, only murals in the triple arch area of the North Mosque were analyzed, and further investigation into the restoration dates of other murals in the North Mosque is required.

The decorative motifs in the North Mosque, notable for their distinct Chinese characteristics, were created using traditional Chinese mural materials and techniques. These observations exemplify the cross-cultural exchange and mutual influence in the field of art. Moreover, the North Mosque murals serve as important and reliable physical evidence for studying cultural exchanges.

5. Conclusions

The preservation of cultural heritage holds immense significance, necessitating a thorough comprehension of the materials utilized by artists and artisans in bygone eras. In this research, we employed a combination of diverse techniques to examine the materials employed in the wall paintings of the North Mosque, offering a compelling instance of multi-method analysis. Moreover, our study underscored the indispensable necessity and the importance of integrating multiple analytical approaches when investigating cultural heritage materials. Through our findings, it was revealed that ancient painters and craftsmen employed both traditional Chinese pigments and imported synthetic pigments in the embellishment of the sacred building. This research not only corroborated and supplemented previous studies on the subject, but also enriched the expertise of restoration professionals while addressing the dearth of historical restoration information.

Author Contributions: Conceptualization, S.D. and L.L.; methodology, S.D. and L.L.; software, S.D. and J.X.; formal analysis, S.D., J.J. and Y.W.; investigation, S.D., J.X. and G.Z.; data curation, S.D., J.X. and P.F.; writing—original draft preparation, S.D.; writing—review and editing, L.L.; supervision, S.D. and L.L.; project administration, L.L.; funding acquisition, J.H. All authors have read and agreed to the published version of the manuscript.

Funding: This research was funded by National Key R&D Program of China (grant number: 2020YFC1522500).

Institutional Review Board Statement: Not applicable.

Informed Consent Statement: Not applicable.

Data Availability Statement: Not available.

Acknowledgments: The authors would like to thank Zhan Wang and Xiaojuan Dang for their support of this study. The authors thank the Reviewers and the Editors for all comments and suggestions, which helped them to improve the quality of the article.

Conflicts of Interest: The authors declare no conflict of interest.

References

1. Gao, Z.F. The historical causes and practical considerations of the development of the sinicization of Islam. *China Relig.* **2023**, *278*, 57–59.
2. Liu, X.C. Traits of the Muslims of China based on census data analysis. *J. Hui Muslim Minor. Stud.* **2014**, *24*, 70–76. [CrossRef]
3. Sun, G. Architectural features of Mosque buildings in China. *J. Hebei Eng. Tech. Coll.* **2017**, *1*, 45–49. [CrossRef]
4. Huo, S.Q.; Mei, D.M. A study of the philosophical thinking of the Qur'an. *J. Hui Muslim Minor. Stud.* **2016**, *3*, 121–124. [CrossRef]
5. Ding, C.; Li, Y.Q.; Wang, D. Study on Architectural Features of Traditional Mosque in Jinan. *J. Hefei Univ. Technol. (Soc. Sci.)* **2017**, *31*, 109–114. [CrossRef]
6. Wang, T.M.; Qi, M. The development of mosques in small gathering areas of the Hui people—The case of Linqing, Shandong province. *Yi Hai* **2014**, *251*, 168–170. [CrossRef]
7. Cultural relics of the Grand Canal in Linqing. *Chunqiu Birmonthly* **2016**, *75*, 2.
8. Dao, W. Shandong Linqing Mosque, the wonderful art of mosque architecture. *China Muslim* **2006**, *4*, 35–36.
9. Doménech, C.; María, T.; Osete, C.L. Another beauty of analytical chemistry: Chemical analysis of inorganic pigments of art and archaeological objects. *Chemtexts* **2016**, *2*, 14. [CrossRef]
10. Ajò, D.; Casellato, U.; Fiorin, E.; Vigato, P.A. Ciro Ferri's frescoes: A study of painting materials and technique by SEM-EDS microscopy, X-ray diffraction, micro FT-IR and photoluminescence spectroscopy. *J. Cult. Herit.* **2004**, *5*, 333–348. [CrossRef]
11. Mona, A.G. Multidisciplinary study of a Qajar lacquered painting: Technology and materials characterization. *Vib. Spectrosc.* **2022**, *119*, 103355. [CrossRef]

12. Jennifer, P.; Mark, K.; Margaret-Ashley, V. Direct Inlet Py-GC-MS analysis of cultural heritage materials. *J. Anal. Appl. Pyrolysis* **2022**, *164*, 105506. [CrossRef]
13. Shen, J.; Li, L.; Zhang, D.D.; Dong, S.H.; Xiang, J.K.; Xu, N. A Multi-analytical approach to investigate the polychrome clay sculpture in Qinglian temple of Jincheng, China. *Materials* **2022**, *15*, 5470. [CrossRef]
14. He, J.; Zhou, W.Q.; Hu, D.B.; Liu, S.J.; Otero, J.; Carlos, R.N. A multi-analytical approach for the characterization of materials, manufacturing process and damage mechanisms of wall paintings in Samye Temple, Tibet. *Dye Pigment.* **2022**, *207*, 110704. [CrossRef]
15. Wang, J.Y.; Wei, L.; Liu, Z.J. Raman Spectra of Some Mineral Pigments Used in Ancient Chinese Artworks. *J. Light Scatt.* **2012**, *1*, 86–91. [CrossRef]
16. Liu, Z.J.; Wang, J.Y.; Han, G.L.; Zhou, X. Raman spectra of some mineral pigments used in ancient Chinese artworks (II). *J. Light Scatt.* **2013**, *2*, 170–175. [CrossRef]
17. Goodall, R.A.; Hall, J.; Viel, R.; Fredericks, P.M. A spectroscopic investigation of pigment and ceramic samples from Copán, Honduras. *Archaeometry* **2009**, *51*, 95–109. [CrossRef]
18. Melo, H.; Cruz, A.; Candeias, A.; Mirão, J.; Cardoso, A.M.; Oliveira, M.J.; Valadas, S. Problems of analysis by FTIR of calcium sulphate-based preparatory layers: The case of a group of 16th-century Portuguese paintings. *Archaeometry* **2014**, *56*, 513–526. [CrossRef]
19. Mandal, P.K.; Mandal, T.K. Anion water in gypsum ($CaSO_4 \cdot 2H_2O$) and hemihydrate ($CaSO_4 \cdot 1/2H_2O$). *Cem. Concr. Res.* **2002**, *32*, 313–316. [CrossRef]
20. Derrick, M.R.; Stulik, D.; Landry, J.M. *Infrared Spectroscopy in Conservation Science*; The Getty Conservation Institute: Los Angeles, CA, USA, 1999.
21. Frost, R.L. Raman and FTIR spectroscopy of natural oxalates: Implications for the evidence of life on Mars. *Chin. Sci. Bull.* **2003**, *48*, 1844–1852. [CrossRef]
22. Trovão, J.; Gil, F.; Catarino, L.; Soares, F.; Tiago, I.; Portugal, A. Analysis of fungal deterioration phenomena in the first Portuguese King tomb using a multi-analytical approach. *Int. Biodeterior. Biodegrad.* **2020**, *149*, 104933. [CrossRef]
23. Bruni, S.; Cariati, F.; Casadio, F.; Toniolo, L. Spectrochemical characterization by micro-FTIR spectroscopy of blue pigments in different polychrome works of art. *Vib. Spectrosc.* **1999**, *20*, 15–25. [CrossRef]
24. Tarling, S.E.; Barnes, P.; Klinowski, J. The structure and Si, Al distribution of the ultramarines. *Acta Crystallogr. Sect. B Struct. Sci.* **1988**, *44*, 128–135. [CrossRef]
25. Esteban, C.P.; Regino, S.P.; Adrián, G.H.; Julio, R.P. Cluster ordering in synthetic ultramarine pigments. *Microporous Mesoporous Mater.* **2008**, *116*, 344–351. [CrossRef]
26. Clark, R.; Franks, M.L. The resonance Raman spectrum of ultramarine blue. *Chem. Phys. Lett.* **1975**, *34*, 69–72. [CrossRef]
27. Clark, R.; Dines, T.J.; Kurmoo, M. On the nature of the sulfur chromophores in ultramarine blue, green, violet, and pink and of the selenium chromophore in ultramarine selenium: Characterization of radical anions by electronic and resonance Raman spectroscopy and the determination of their excited-state geometries. *Inorg. Chem.* **1983**, *22*, 2766–2772. [CrossRef]
28. Osticioli, I.; Mendes, N.F.C.; Nevin, A.; Gil, F.P.S.C.; Becucci, M.; Castellucci, E. Analysis of natural and artificial ultramarine blue pigments using laser induced breakdown and pulsed Raman spectroscopy, statistical analysis and light microscopy. *Spectrochim. Acta Part A Mol. Biomol. Spectrosc.* **2009**, *73*, 525–531. [CrossRef]
29. Gerhard, P. Ultramarine pigments. *Phys. Sci. Rev.* **2021**, *6*, 879–885. [CrossRef]
30. Wang, J.Y. The study on composed ultramarine of Dunhuang grottoes. *Dunhuang Res.* **2000**, *1*, 76–81.
31. Lei, Z.B.; Wu, W.; Shang, G.H.; Wu, Y.Q.; Wang, J.L. Study on colored pattern pigments of a royal Taoist temple beside the Forbidden City (Beijing, China). *Vib. Spectrosc.* **2017**, *92*, 234–244. [CrossRef]
32. Gao, F.; Zhou, X.; Zhou, H.; Li, M.Y.; Tong, H.; Liu, S.J. Characterization and analysis of sandstone substrate, mortar layers, gold foils, and paintings of the Avalokitesvara Statues in Dazu County (China). *J. Cult. Herit.* **2016**, *21*, 881–888. [CrossRef]
33. Wang, X.; Zhen, G.; Hao, X.Y.; Zhou, P.; Wang, Z.; Jia, J.; Gao, Y.; Dong, S.H.; Tong, H. Micro-Raman, XRD and THM-Py-GC/MS analysis to characterize the materials used in the Eleven-Faced Guanyin of the Du Le Temple of the Liao Dynasty, China. *Microchem. J.* **2021**, *171*, 106828. [CrossRef]
34. Rocco, M.; Darinn, C.; Giuseppe, C.; Daniele, F.; He, L.; Silvia, P. Analytical study of traditional decorative materials and techniques used in Ming Dynasty wooden architecture. The case of the Drum Tower in Xi'an, P.R. of China. *J. Cult. Herit.* **2004**, *5*, 273–283. [CrossRef]
35. Fiedler, I.; Bayard, M. Emerald green and Scheele's green. In *Artists' Pigments, A Handbook of Their History and Characteristics*; Fitzhugh, E.W., Ed.; Oxford University Press: Oxford, UK, 1997; Volume 3, pp. 249–251.
36. Gulyaev, R.V.; Kryuchkova, N.A.; Mazalov, L.N.; Boronin, A.I.; Basova, T.V.; Plyashkevich, V.A. X-ray photoelectron investigation of charge distribution in copper(II) phthalocyanine complexes. *J. Surf. Investig.* **2011**, *5*, 48–56. [CrossRef]
37. Castillejo, M.; Martin, M.; Silva, D.; Stratoudaki, T.; Anglos, D.; Burgio, L.; Clark, R.J.H. Laser-Induced breakdown spectroscopy and Raman microscopy for analysis of pigments in polychromes. *J. Cult. Herit.* **2000**, *1*, 297–302. [CrossRef]
38. Shen, A.G.; Wang, X.H.; Xie, W.; Shen, J.; Li, H.Y.; Liu, Z.A.; Hu, J.M. Pigment identification of colored drawings from Wuying Hall of the imperial palace by Micro-Raman Spectroscopy and Energy Dispersive X-Ray Spectroscopy. *J. Raman Spectrosc.* **2006**, *37*, 230–234. [CrossRef]

39. Lombardo, C.C. *Forever Gothic? Analysis and Interpretation of the Interior of the Great North Bedchamber at Strawberry Hill*; University of Pennsylvania: Philadelphia, PA, USA, 2006; pp. 91–92.
40. Yu, F.A. *Chinese Painting Colours: Studies of Their Preparation and Application in Traditional and Modern Times*; Silbergeld, J.; McNair, A., Translators; University of Washington Press: Washington, DC, USA, 1988.
41. Cheng, X.L.; Xia, Y.; Ma, Y.R.; Lei, Y. Three fabricated pigments (Han purple, indigo and emerald green) in ancient Chinese artifacts studied by Raman microscopy, energy-dispersive X-ray spectrometry and polarized light microscopy. *J. Raman Spectrosc.* **2010**, *38*, 1274–1279. [CrossRef]
42. Stanzani, E.; Bersani, D.; Lottici, P.P.; Colomban, P. Analysis of artist's palette on a 16th century wood panel painting by portable and laboratory Raman instruments. *Vib. Spectrosc.* **2016**, *85*, 62–70. [CrossRef]
43. Burgio, L.; Clark, R.J.H. Library of FT-Raman spectra of pigments, minerals, pigment media and varnishes, and supplement to existing library of Raman spectra of pigments with visible excitation. *Spectrochim. Acta Part A Mol. Biomol. Spectrosc.* **2001**, *57*, 1491–1521. [CrossRef]
44. Zhou, G.X. Cinnabar in China and Its development in function. *Dunhuang Res.* **2010**, *120*, 51–59. [CrossRef]
45. Ma, Q.L.; Hu, Z.D.; Li, Z.X.; Liang, B.L. Analysis of pigments and block pigments from painted pottery excavated from the Dadiwan site, Qin'an, Gansu. *Cult. Relics* **2001**, *08*, 84–92+1.
46. Zhu, T.Q.; Chen, J.; Hui, R.; Gong, L.; Zhang, W.H.; Zhang, Y.C. Spectroscopic characterization of the architectural painting from the Cizhong Catholic Church of Yunnan Province, China. *Anal. Lett.* **2013**, *46*, 2253–2264. [CrossRef]
47. Van Der Weerd, J.; Smith, G.D.; Firth, S.; Clark, R.J.H. Identification of black pigments on prehistoric southwest American potsherds by infrared and Raman microscopy. *J. Archaeol. Sci.* **2004**, *31*, 1429–1437. [CrossRef]
48. Zhang, X.H. Chinese Traditional pigment minerals. *China Non-Met. Miner. Ind.* **2020**, *142*, 10–14. [CrossRef]
49. Chiavari, G.; Galletti, G.C.; Lanterna, G.; Mazzeo, R. The potential of pyrolysis—Gas chromatography/mass spectrometry in the recognition of ancient painting media. *J. Anal. Appl. Pyrolysis* **1993**, *24*, 227–242. [CrossRef]
50. Wang, N.; Gu, A.; Qu, Y.J.; Lei, Y. Identification of polysaccharide binding materials used in cultural relics by pyrolysis-gas chromatography/mass spectrometry. *Chin. J. Chromatogr.* **2022**, *40*, 753–762. [CrossRef]
51. Wang, N.; Gu, A.; Min, J.R.; Li, G.H.; Lei, Y. Thermal cleavage of commonly used protein-based cementing materials in cultural relics by pyrolysis-gas chromatography/mass spectrometry. *Chin. J. Anal. Chem.* **2020**, *48*, 90–96.

Disclaimer/Publisher's Note: The statements, opinions and data contained in all publications are solely those of the individual author(s) and contributor(s) and not of MDPI and/or the editor(s). MDPI and/or the editor(s) disclaim responsibility for any injury to people or property resulting from any ideas, methods, instructions or products referred to in the content.